

Article

Bio-Based *Eucommia ulmoides* Gum Composites with High Electromagnetic Interference Shielding Performance

Hailan Kang ^{1,2} , Sen Luo ^{1,2}, Hongyang Du ^{1,2}, Lishuo Han ^{1,2}, Donghan Li ^{1,2}, Long Li ^{1,2,*} and Qinghong Fang ^{1,2,*}

¹ College of Materials Science and Engineering, Shenyang University of Chemical Technology, Shenyang 110142, China; kanghailan@syuct.edu.cn (H.K.); luosen971012@163.com (S.L.); 13940204549@163.com (H.D.); hanls0022@163.com (L.H.); lidonghansyuct@126.com (D.L.)

² Key Laboratory for Rubber Elastomer of Liaoning Province, Shenyang University of Chemical Technology, Shenyang 110142, China

* Correspondence: lilong@syuct.edu.cn (L.L.); fqh80@126.com (Q.F.); Tel.: +86-189-0092-6770 (L.L.); +86-138-4010-2035 (Q.F.)

Abstract: Herein, high-performance electromagnetic interference (EMI) shielding bio-based composites were prepared by using EUG (*Eucommia ulmoides* gum) with a crystalline structure as the matrix and carbon nanotube (CNT)/graphene nanoplatelet (GNP) hybrids as the conductive fillers. The morphology of the CNT/GNP hybrids in the CNT/GNP/EUG composites showed the uniform distribution of CNTs and GNPs in EUG, forming a denser filler network, which afforded improved conductivity and EMI shielding effect compared with pure EUG. Accordingly, EMI shielding effectiveness values of the CNT/GNP/EUG composites reached 42 dB in the X-band frequency range, meeting the EMI shielding requirements for commercial products. Electromagnetic waves were mainly absorbed via conduction losses, multiple reflections from interfaces and interfacial dipole relaxation losses. Moreover, the CNT/GNP/EUG composites exhibited attractive mechanical properties and high thermal stability. The combination of excellent EMI shielding performance and attractive mechanical properties render the as-prepared CNT/GNP/EUG composites attractive candidates for various applications.

Keywords: *Eucommia ulmoides* gum; carbon nanotubes; graphene; electromagnetic shielding



Citation: Kang, H.; Luo, S.; Du, H.; Han, L.; Li, D.; Li, L.; Fang, Q. Bio-Based *Eucommia ulmoides* Gum Composites with High Electromagnetic Interference Shielding Performance. *Polymers* **2022**, *14*, 970. <https://doi.org/10.3390/polym14050970>

Academic Editor: Ahmed I. A. Abd El-Mageed

Received: 14 January 2022

Accepted: 26 February 2022

Published: 28 February 2022

Publisher's Note: MDPI stays neutral with regard to jurisdictional claims in published maps and institutional affiliations.



Copyright: © 2022 by the authors. Licensee MDPI, Basel, Switzerland. This article is an open access article distributed under the terms and conditions of the Creative Commons Attribution (CC BY) license (<https://creativecommons.org/licenses/by/4.0/>).

1. Introduction

With the widespread application of advanced electronic devices, our lives are enhanced by ever greater convenience. However, the development of electronic devices has created considerable quantities of electromagnetic (EM) pollution due to electromagnetic radiation and EM interference; this pollution affects human health and the normal operation of other devices [1–6]. In order to avoid these issues, many novel materials with high EMI shielding performance were explored with the aim of addressing problems related to EMI and radiation [7]. Conductive polymer composites (CPCs) consisting of polymer and conductive fillers were explored as promising alternative EMI shielding materials; these materials are generally metal-based materials [8–12]. Research on CPCs was motivated by their low weight, flexibility, resistance to corrosion and good processability [13–16].

Numerous efforts were devoted to the design and construction of CPCs using compounding polymers with carbon-based nanofillers, such as carbon black (CB), carbon fibers (CFs), carbon nanotubes (CNTs) and graphene [17–23]. For example, Cheng et al. [24] prepared CPCs using an ultrahigh-molecular-weight polyethylene/polypropylene (PP) blend with conductive CB, which exhibits an absorption-dominated EMI shielding effectiveness (EMI SE) as high as 27.29 dB over the X-band frequency range. Lin et al. [25] developed CF/PP composites with an EMI SE of ~20 dB via adding 15 wt% CFs. Since both CNTs and graphene have exceptional mechanical, electric transport properties and extremely high

aspect ratios, they make excellent conducting fillers in CPCs for EMI shielding applications [26–31]. Wu et al. [32] prepared CNT/PP composites with an EMI SE of 43.1 dB by adding 5 wt% CNTs. Abraham et al. [33] produced CNT/styrene-butadiene rubber composites with ionic liquids, and the EMI SE of the composites was found to reach 35.06 dB at 18 GHz when adding 10 wt% CNTs. Lu et al. [34] fabricated graphene nanoplatelet (GnP)/ethylene propylene diene monomer rubber (EPDM) composites via a combination process that included mixing, ultrasonication and compression. The GnP/EPDM composites exhibit a high EMI SE of 33 dB in the range 8.2–12.4 GHz and 35 dB in the range 12.4–18 GHz.

The EMI shielding performance of CPCs is heavily dependent on the conductivity, dispersion and connectivity of fillers in the matrix [35,36]. Three-dimensional (3D) hybrid filler materials were successfully constructed via the hybridization of one-dimensional (1D) CNTs with two-dimensional (2D) graphene, which can overcome the problem of dispersion faced by the individual fillers. The π - π interaction between the CNTs and the graphene is beneficial in the nanoscale separation of the individual CNTs and graphene sheets [37,38]. Moreover, the long CNTs were found to be entangled with the graphene nanosheet, which inhibited their aggregation and provided efficient pathways for electron transfer. Zhao et al. [39] produced a material with an improved EMI shielding performance using polydimethylsiloxane with CNT/graphene hybrids; this material achieved an EMI SE of 31 dB. Kim et al. [40] fabricated CNT/GnP/PP composites with an EMI SE of 36.5 dB at 1.25 GHz. Mohammed et al. [41] prepared PP/polyethylene composites using GnP/CNT hybrid nanofillers. Across this research, it can be seen that using CNTs and graphene as hybrid fillers yield an effective route to the fabrication of CPCs with excellent EMI shielding performance.

With concern regarding the price fluctuations of fossil fuel reserves and the increasing environmental awareness, eco-friendly polymeric materials have attracted increasing research attention. *Eucommia ulmoides* gum (trans-1,4-polyisoprene, EUG) is extracted from the *Eucommia ulmoides* Oliv and an isomer of natural rubber. Due to its unique dual nature combining properties of both plastics and rubber, EUG was used as a thermoplastic material, thermoelastic shape memory material and as a highly elastic material in many fields. To date, there is little research regarding the use of EUG as an EMI shielding matrix. In the present work, we used EUG with a crystalline structure as a matrix material and CNT/GnP hybrids as conductive fillers to construct a shielding composite with a high EMI shielding performance. The effect of the CNT/GnP hybrids on the morphology, electrical conductivity and EMI shielding properties was investigated. Furthermore, the EMI shielding mechanism of the CNT/GnP/EUG composites was analyzed.

2. Materials and Methods

2.1. Materials

Eucommia ulmoides gum (EUG) was supplied by Shandong Beilong *Eucommia* Chemical Industry Co., Ltd., Weifang, China. Carbon nanotubes (CNTs, with a diameter in the range of 8–15 nm and length of 1–10 μ m) were purchased from the Shanghai Kajite Chemical Technology Co., Ltd., Shanghai, China. Graphene nanosheets (GNPs) were provided by Shenzhen Hongda Changjin Technology Co., Ltd., Shenzhen, China. Triton X-100 (polyethylene glycol tert-octylphenyl ether) used in this work was provided by Shanghai Youdao Aoba Chemical Co., Ltd., Shanghai, China.

2.2. Methods

2.2.1. Preparation

CNTs and GNPs were modified via the use of Triton X-100. An amount of 0.1 g of GNPs (or CNTs) was mixed with 1 mL of Triton X-100 and subsequently grounded manually in an agate bowl for 30 min. The product was then dispersed in deionized water and magnetically stirred in a glass beaker for 20 min. The suspension was ultrasonicated for 60 min in ice bath conditions, filtrated and vacuum dried to obtain *m*-GNPs (or *m*-CNTs).

The calculated amounts of *m*-GNPs (0 wt%, 0.80 wt%, 2.35 wt% and 3.85 wt%) and *m*-CNTs (9.62 wt%) were dispersed in toluene at 2 mg/mL under the action of mechanical stirring; this was followed by sonication for 60 min. The *m*-GNPs and *m*-CNTs suspensions were subsequently mechanically stirred for 10 min and ultrasonicated for 30 min. Then CNT/GNP suspension was added to the EUG toluene solution; the mixture was then mechanically stirred for 30 min and ultrasonicated for 2 h. The mixture was precipitated using ethanol and then dried at 40 °C. The dried mixture was mixed with curing agents (ZnO, 4 phr; SA, 2 phr; sulfur, 2 phr; NOBS, 1.2 phr) on a two-roll mill at 65 °C. Then, the blends were cured into 1-mm-thick sheets under 150 °C at the vulcanization time. The CNT/GNP/EUG composites are referred to as ECG_x, where x represents the content of GNPs added to the composites.

2.2.2. Characterization

The morphology of the composites was investigated via scanning electron microscopy (SEM, SU8010, Hitachi Co., Ltd., Tokyo, Japan) and transmission electron microscopy (TEM, FEI Talos F200, Thermo Fisher Scientific Inc, Shanghai, China). The samples used for SEM were fractured in liquid nitrogen and had a surface coated with a thin gold layer. The TEM samples were ultramicrotomed at −100 °C to produce sections with a thickness in the range of 50–60 nm. Dynamic mechanical rheology measurements were performed using a rubber process analyzer (RPA-8000, Gotech Testing Machines Co., Ltd., Qingdao, China). A strain sweep was undertaken from 1% to 200% at 60 °C and 1 Hz.

The electrical conductivity of the composites was measured using a four-probe conductometer (RTS-9, Guangzhou Four-Probes Technology Co. Ltd., Guangzhou, China). The EMI shielding performance of the composites was measured in the frequency range of 8.2–12.4 GHz (X band) at room temperature, using a vector network analyzer (E5071C, Agilent Technologies, Santa Clara, CA, USA); the test samples were of length 22.86 mm, width 10.16 mm and thickness 2.00 mm. The EMI performance parameters, including the SE total (SE_T), SE reflection (SE_R) and SE absorption (SE_A), were calculated from the scattering parameters (S_{11} and S_{21}).

$$R = |S_{11}|^2 \quad (1)$$

$$T = |S_{21}|^2 \quad (2)$$

$$SE_R = -\log_{10}(1 - R) \quad (3)$$

$$SE_A = -\log_{10}(T/(1 - R)) \quad (4)$$

$$SE_T = SE_R + SE_A \quad (5)$$

The tensile tests were carried out using an INSTRON 3365 testing machine (Instron Co., Ltd., Norwood, MA, USA) according to the standard ASTM D412 using a crosshead speed of 500 mm/min at 23 ± 2 °C. Cut the EUG/CNTs/GNPs composite sample into strips with a section width of 6 mm and thickness of 2 mm with a dumbbell cutter, and clamp both ends of each sample. For each data point, at least five specimens were tested, and an average value was taken. The thermal stability of the samples was measured via thermogravimetric analysis (TGA, Q50, TA Instruments, Rutherfordton, NC, USA) from 40 °C to 600 °C using a heating rate of 10 °C/min in an N₂ atmosphere. Differential scanning calorimetric (DSC) measurements were obtained using a DSC-Q200 (TA Instruments, Rutherfordton, NC, USA) under N₂ from −70 °C to 100 °C at a heating/cooling rate of 10 °C/min. The crystallinity of the EUG was determined, as

$$X_c = \frac{\Delta H_m}{\Delta H_m^*} \times 100\% \quad (6)$$

where ΔH_m^* is the theoretical value of 100% crystallized EUG (125.6 J/g).

3. Results and Discussion

3.1. The Morphology of the CNT/GNP/EUG Composites

It is generally accepted that the properties of composite material are closely correlated with the dispersion of the filler material used. Figures 1 and 2 show the SEM and TEM images of CNT/GNP/EUG composites. As shown in Figures 1a and 2a, the CNTs are uniformly dispersed within the EUG matrix without obvious agglomeration or entanglement. As shown in Figures 1b–d and 2b, the CNTs and GNPs are uniformly dispersed across the matrix after the shear force was applied during the open mill process. CNTs were observed to show an individual distribution state and are seen to be closely attached to the GNPs, further demonstrating that the GNPs lead to an efficient dispersion of the CNTs and implying that there exists a high-strength binding interaction between the GNPs and CNTs. Because of the π - π interaction between the CNTs and GNPs, GNPs can improve the dispersibility of CNTs and inhibit their re-aggregation due to their larger surface area and steric hindrance; rod-shaped CNTs can also reduce stacking effects of the GNPs [42]. Furthermore, with an increase in hybrid loading, the GNPs exhibit increased agglomeration; these were caused by the effect of the π - π bond between the GNPs and the strong Van der Waals force. Thus, the composites form a more complete CNT/GNP conductive network, which provides a favorable condition for the electrical conductivity of the composites.

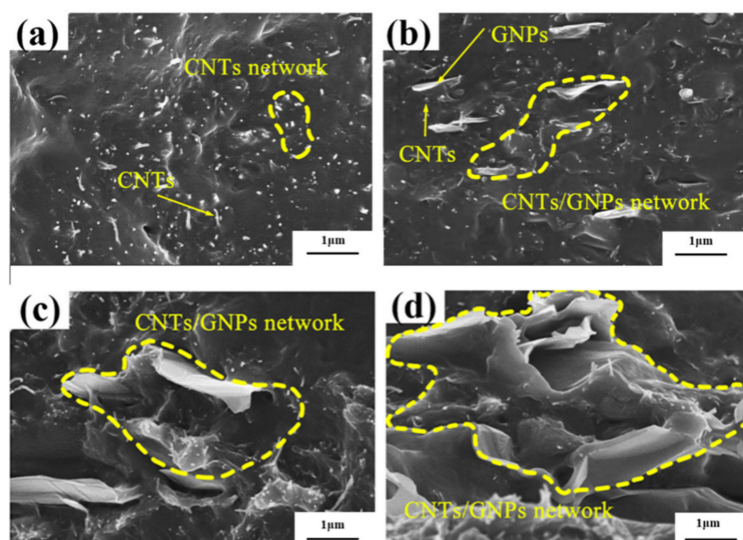


Figure 1. SEM images of CNT/GNP/EUG composites: (a) ECG0; (b) ECG1; (c) ECG2; (d) ECG3.

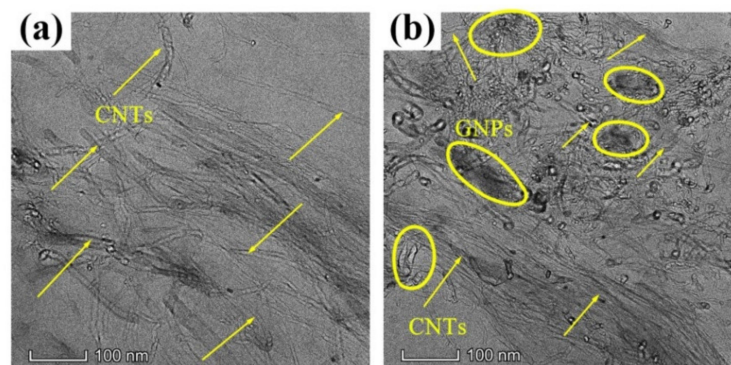


Figure 2. TEM images of CNT/GNP/EUG composites: (a) ECG0; (b) ECG3.

The Payne effect is widely used to characterize filler dispersion and filler networks. Figure 3 shows the storage modulus (G') as a function of the strain for the CNT/GNP/EUG composites. G' of the CNT/GNP/EUG composites is seen to decrease rapidly with in-

creasing dynamic strain amplitudes; it is also seen to exhibit high sensitivity to strain, an indication of a typical Payne effect. The decrease in G' is due to the destruction of filler networks. G' increases significantly with increasing GNP loading of the CNT/GNP hybrids, demonstrating that denser filler networks are formed between CNTs and GNPs at higher CNT/GNP loading. The difference between G' at 200% and G' at 1% (referred to as $\Delta G'$) also increases with the increase in the GNP loading; this phenomenon indicates an increase in the Payne effect. In summary, with increasing GNP loading within CNT/GNP hybrids, the filler networks possess a higher modulus and a higher sensitivity to strain. The strong filler networks also demonstrate that the CNT/GNP hybrids are highly dispersed within the EUG matrix.

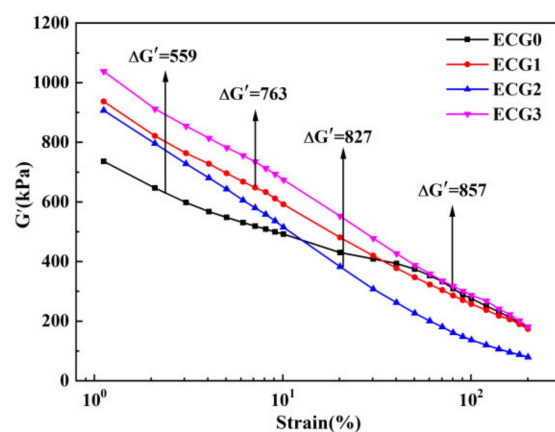


Figure 3. Storage modulus versus strain of CNT/GNP/EUG composites.

3.2. Electrical Conductivity and EMI Shielding Properties of the CNT/GNP/EUG Composites

Electrical conductivity is a key factor that determines the EMI shielding properties of a given composite [43]. Materials with high electrical conductivity usually exhibit good EMI shielding properties. The volume electrical conductivity values of the CNT/GNP/EUG composites fabricated here are shown in Figure 4. CNTs are observed to be non-directionally dispersed and distributed but in a directional distribution in local microbeams, which results in the composites having anisotropic characteristics across different micro-domains; these properties have an effect on the electrical conductivity of the rubber. The electrical conductivity of CNTs/EUG composites with 9.62 wt% CNTs is seen to be around 2.31 S/cm. This result indicates that the CNTs in the composites form a conductive network at this CNT loading. The electrical conductivity of the CNT/GNP/EUG composites slightly increases with increasing of GNP loading within CNT/GNP hybrids. As shown in Figure 2, the CNT/GNP hybrids were well dispersed within the EUG matrix, which is conducive to the formation of perfect conductive networks and leads to an improved EMI shielding performance.

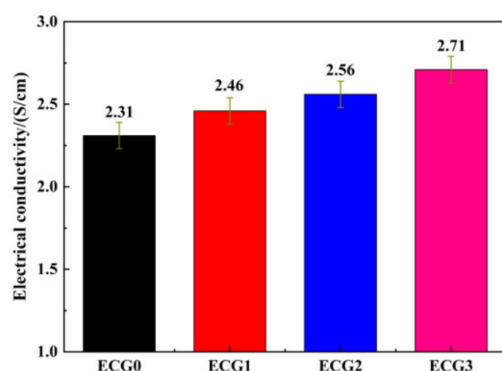


Figure 4. Electrical conductivity of CNT/GNP/EUG composites.

The outstanding electrical properties endow CNT/GNP/EUG composites with high EMI shielding properties [44]. The EMI shielding properties of the CNT/GNP/EUG composites were assessed by measuring the values of SE_T , SE_R and SE_A . Figure 5 shows the EMI SE_T , SE_R and SE_A of the CNT/GNP/EUG composites in the X-band frequency range. The pure EUG exhibits a very small SE_T value of less than 0.5 dB, indicating that EUG is almost completely transparent to the electromagnetic waves over the whole X-band frequency range. It can be seen from Figure 5a that the value of SE_T of the CNT/GNP/EUG composites gradually increased from 30.29 dB to 42.49 dB with the increase in the GNPs loading within the CNT/GNP hybrids. The enhanced EMI shielding properties are attributed to the increased conductive networks created by the synergistic effect of GNPs and CNTs.

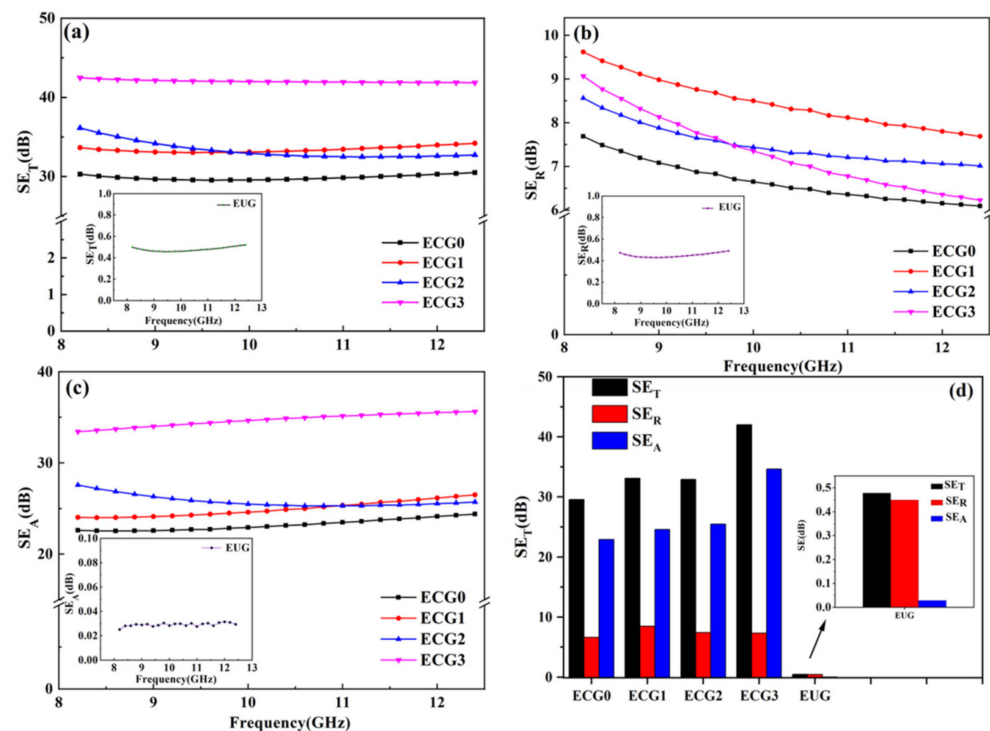


Figure 5. (a) EMI SE_T (b) EMI SE_R , (c) EMI SE_A and (d) EMI SE_T at 10 GHz of CNT/GNP/EUG composites.

In order to state the synergistic effect of 2D GNPs and 1D CNTs, the same weight loading of GNP and CNT composites were fabricated, and the comparative results of electrical conductivity and EMI shielding efficiency are summarized in Figure 6. The electrical conductivity and EMI SE_T of the CNT/GNP/EUG composite are all higher than CNT/EUG composite and GNP/EUG composite. As a 1D material, CNTs contact each other predominantly through point contacts. As a 2D material, GNPs contact each other via surface contacts. In CNT/GNP hybrids, GNPs function as the ‘spacers’ between the polymers, and the CNTs function as the ‘wires’ making up the conductive network. The combination of the two fillers creates much denser conductive networks than either filler used alone. Such perfect conductive networks permit the dissipation of electromagnetic waves through both reflection and absorption. Therefore, the CNT/GNP/EUG composites exhibit enhanced electrical conductivity and EMI shielding efficiency because of the synergistic effect of GNP and CNTs.

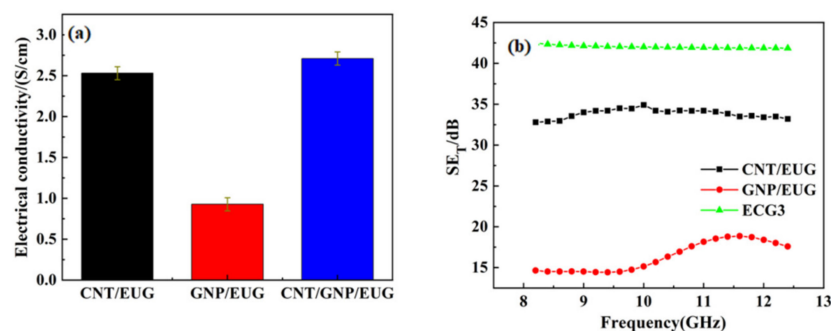


Figure 6. Comparison of (a) electrical conductivity and (b) EMI SE_T of CNT/EUG composite (13.47 wt% CNT), GNP/EUG composite (13.47 wt% GNP) and CNT/GNP/EUG composite (9.62 wt% CNT and 3.85 wt% GNP, ECG3).

The maximum EMI SE_T value of the CNT/GNP/EUG composite is seen to be as high as ~42 dB, a value that meets the EMI shielding requirement for commercial products. Table 1 compares the results obtained in this work with other EMI shielding polymeric composites reported in previous work [17,18,20,28,30–32]; it is seen that the CNT/GNP/EUG composites created in this work exhibit superior EMI SE_T compared with previously studied composites. The results indicate that this work provides a practical and effective method for the preparation of high-performance EUG-based EMI shielding composites.

Table 1. Comparison of EMI shielding properties of CNT/GNP/EUG composites with other CPCs.

Materials	Carbon Filler Contents	Thickness (mm)	SE (dB)	Frequency Range	Ref.
CB/Silicone Rubber	15 phr	2.0	20	0.01–10,000 MHz	[17]
CF/MWCNT/PBT/PolyASA	8 vol % + 2 vol %	2.0	33.7	8.2–12.4 GHz	[18]
CNT/PE	10 wt%	3.0	35	0.5–1.5 GHz	[20]
RGO/CB/PDMS	15 wt% + 17 wt%	1.5	28	8.2–18 GHz	[28]
graphene/SBR	27.81 wt%	3.0	45	8–12 GHz	[30]
GN/NBR	4 wt%	2.0	77	1–12 GHz	[31]
CNTs/RGO/Epoxy	0.83 wt% + 1.2 wt%	3	42	8.2–12.4 GHz	[32]
CNTs/GNPs/EUG	9.62 wt% + 3.85 wt%	2.0	42.5	8.2–12.4 GHz	this work

PBT: Polyb; PBT: Polybutylene terephthalate; ASA: Acrylonitrile Styrene acrylate copolymer; PDMS: Polydimethylsiloxane; SBR: 1,3-butadiene polymer.

3.3. EMI Shielding Mechanism of the CNT/GNP/EUG Composites

In order to fully elucidate the EMI shielding mechanism of the CNT/GNP/EUG composites, the values of SE_A , SE_R and the relative values at 10 GHz were calculated and plotted in Figure 5b,c,d, respectively. The values of SE_A and SE_R of the CNT/GNP/EUG composites all increase with increases in GNP loading of the CNT/GNP hybrids. More importantly, the SE_A values greatly increase with the GNP loading of the CNT/GNP hybrids. In all the CNT/GNP/EUG composites, the SE_A values are much greater than the SE_R values; this is because the conductive networks provide a sufficient number of interfaces that form multiple reflections and thus attenuate the incident electromagnetic waves [45]. For instance, the SE_T , SE_R and SE_A of ECG3 are 42 dB, 7.4 dB and 34.6 dB, respectively. Furthermore, the SE_A value that represents absorption makes up 82% of the SE_T value, whereas the SE_R value that represents reflection accounts for only 18% of the SE_T value. Thus, the results of this work indicate that absorption is the predominant shielding mechanism of the CNT/GNP/EUG composites.

The complex permittivity of the CNT/GNP/EUG composites was also measured in order to understand their EM absorption properties better. Figure 7 shows the real part (ϵ'), the imaginary part (ϵ'') and the dielectric loss tangent ($\tan \delta_\epsilon = \epsilon''/\epsilon'$) in the X-band frequency range. The values of ϵ' and ϵ'' represent the storage and loss capability of electric energy within a material, respectively, whereas $\tan \delta_\epsilon$ is used to evaluate the dielectric loss capacity of a material. Both ϵ' and ϵ'' decrease with increasing frequency; this

decrease is related to the interface polarization [46]. It is noted that the values of ϵ' and ϵ'' of the CNT/GNP/EUG composites increase with an increase in the GNP loading of the CNT/GNP hybrids. This is ascribed to the formation of perfect conducting networks by the CNTs and GNPs within the EUG matrix. The enhanced ϵ' value is predominantly due to the creation of more dipoles within the composite. The uniform distribution of the CNT/GNP hybrids without agglomeration can create many interfaces and hence induce polarization at the interfaces of CNT/GNP, CNT/EUG and GNP/EUG. Moreover, the introduction of more layers of GNPs with a large specific surface area induces an increase in the interface polarization [47]. The increase in the value of ϵ'' with an increase in the GNP loading is attributed to the dielectric relaxation and electrical conductivity of the composites. The incorporation of GNPs enhances the electrical conductivity, resulting in high conduction loss. Furthermore, the presence of a high number of interfaces between the EUG matrix and the fillers results in further increases in the dielectric loss within the composite. The value of $\tan \delta_\epsilon$ is significantly increased by increases in GNP loading, indicating a superior dielectric loss capacity. The enhanced value of $\tan \delta_\epsilon$ represents significant dissipation of electrical energy and attenuation of wave absorption.

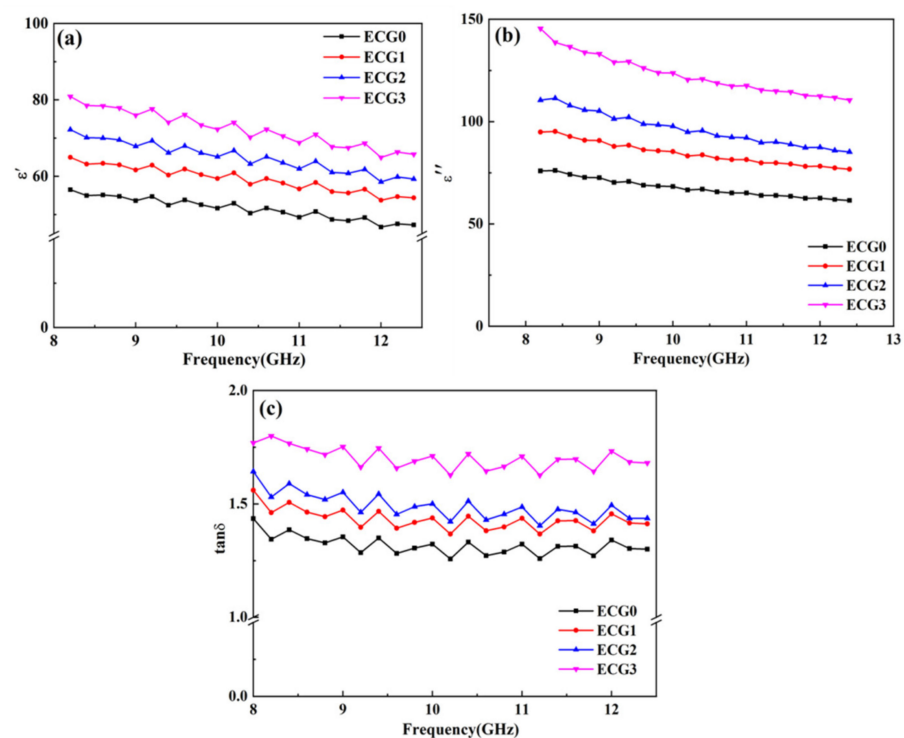


Figure 7. (a) ϵ' , (b) ϵ'' and (c) $\tan \delta_\epsilon$ of CNT/GNP/EUG composites.

Based on the preceding analysis, we established the shielding mechanism of the CNT/GNP/EUG composites, which is illustrated in Figure 8. When the EM waves reach the interfaces within the composite, a proportion of the EM waves are reflected at the surface of the CNT/GNP/EUG composite due to the impedance mismatch between the composites and the air, while a proportion of EM waves is absorbed by the CNT/GNP/EUG composite due to the conduction losses, multiple reflections from interfaces and the interfacial dipole relaxation losses. The CNT/GNP/EUG composites form more effective conductive networks due to the synergistic effect of 2D GNPs and 1D CNTs, thereby causing the attenuation of EM waves via Joule heating, which increases the EM absorption. Moreover, the numerous EUG/CNT, EUG/GNP and CNT/GNP interfaces facilitate substantial attenuation of the EM waves via multiple reflections and scattering. The interfacial polarizations also attenuate EM waves and enhance the EM wave absorption effect. Importantly, the boundary of crystalline–amorphous phases within EUG matrix can accumulate electrical

charges, thus resulting in polarization loss, while the crystalline regions of the EUG matrix also increase the propagation of EM waves within the material and hence enhances EM absorption [48,49].

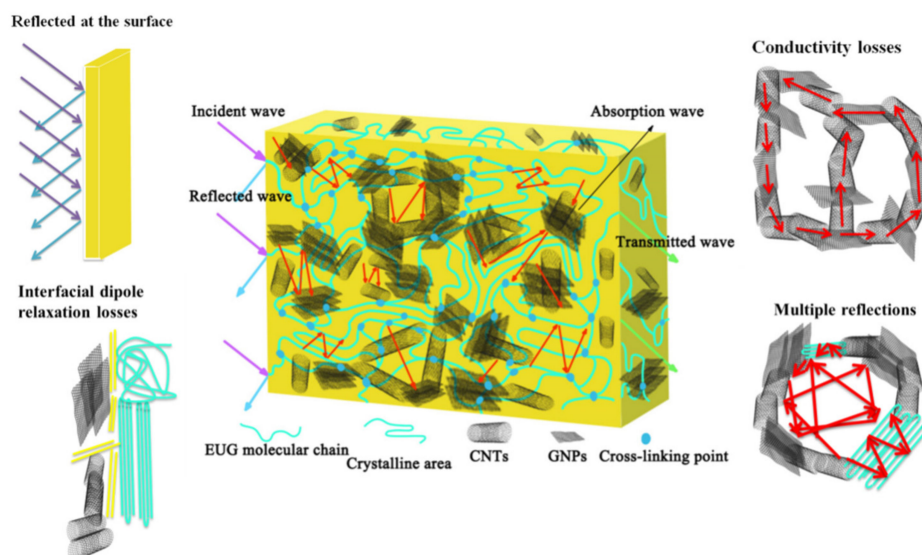


Figure 8. Proposed electromagnetic shielding mechanism for CNT/GNP/EUG composites.

3.4. Crystallinity of the CNT/GNP/EUG Composites

Thermal and crystalline behaviors were characterized by the DSC curves, and the crystallinity of EUG was calculated. As shown in Figure 9a, all samples exhibit one peak upon heating curves, which corresponds to the melting peak of crystalline EUG. Compared with pure EUG, the melting temperature (T_m) of the CNT/EUG composite shifts to a higher temperature, and the melting enthalpy (ΔH_m) increases from -23.95 to -35.48 J/g. Accordingly, the crystallinity (X_c) of the CNT/EUG composite also increases from 19.1% to 28.2%, implying that CNTs acted as the nucleating agent and promoted the crystallization of EUG segments. However, the T_m , ΔH_m and X_c of CNT/GNP/EUG composite all decrease with the increase in GNP loading of the CNT/GNP hybrids. These results indicate that the EUG segmental mobility was restricted by strong networks formed by the synergistic effect of CNTs and GNPs.

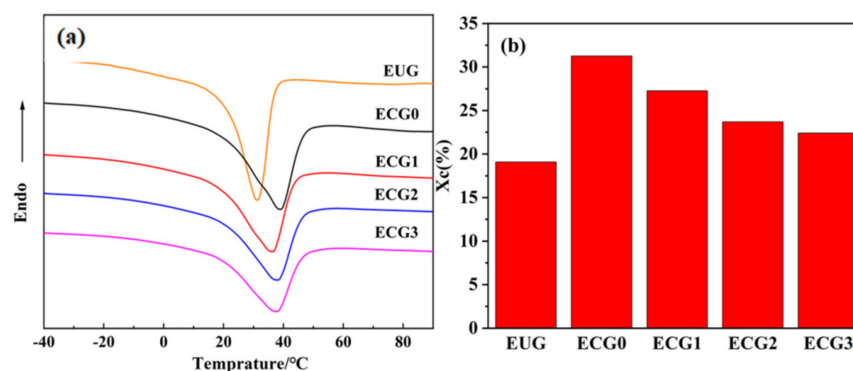


Figure 9. (a) DSC curves of CNT/GNP/EUG composites, (b) the crystallinity (X_c) of CNT/GNP/EUG composites.

3.5. Thermal and Mechanical Properties of the CNT/GNP/EUG Composites

Figure 10 depicts the TGA curves of the CNT/GNP/EUG composites; the related data are shown in Table 2. As shown in Figure 8, the thermal decomposition of CNT/GNP/EUG composites takes place in a single stage between 260 °C and 300 °C, predominantly due

to the pyrolysis of the EUG macromolecules. The decomposition temperatures of the CNT/GNP/EUG composites with 5% and 30% weight loss (T_5 , T_{30}) and the calculated heat resistance index (T_{HRI}) are all higher than 303 °C, 410 °C and 180 °C, respectively. The value of T_{HRI} of the CNT/GNP/EUG composites all increase with the increase in the GNP loading of the CNT/GNP hybrids. The value of T_{HRI} for the CNT/GNP/EUG is 191 °C, which is 11 °C higher than that of pure EUG (180 °C). The reason for this increase is due to the CNT and GNP fillers possessing high heat resistance, which improves the thermal stability of the EUG matrix.

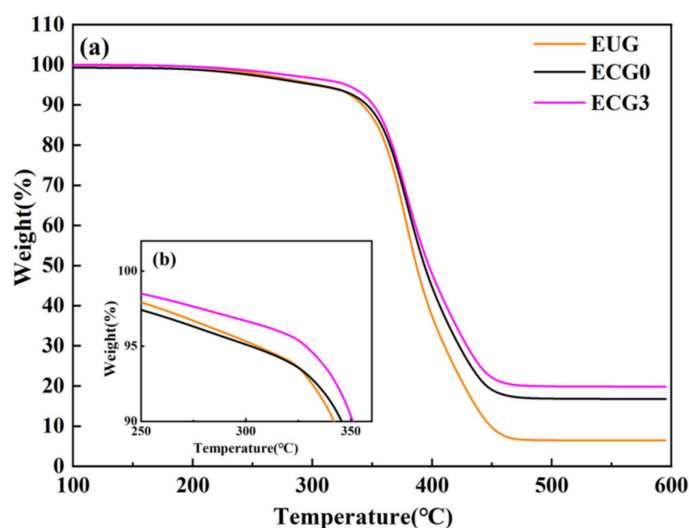


Figure 10. (a) Thermogravimetric curves of CNT/GNP/EUG composites. (b) Enlarged view of thermogravimetry at 100–90%.

Table 2. Thermal characteristics data of CNT/GNP/EUG composites.

Samples	Weight Loss Temperature (°C)		$T_{\text{Heat-resistance index}}$ (°C)
	$T_{d,5\%}$	$T_{d,30\%}$	
EUG	305	410	180
ECG0	303	423	184
ECG3	328	429	191

T_5 and T_{30} correspond to the decomposition temperature of 5% and 30% weight loss, respectively;
 $T_{\text{Heat-resistance index}} = 0.49 * [T_5 + 0.6 * (T_{30} - T_5)]$.

The mechanical properties of the CNT/GNP/EUG composites are shown in Figure 11. The tensile strength of the CNT/GNP/EUG composites is seen to increase with an increase in the GNP loading of the CNT/GNP hybrids. The elongation at break initially increases and subsequently decreases with increasing GNP loading of the composite. The incorporation of GNPs in the CNT/GNP/EUG composite improves the dispersion of CNTs, resulting in enhanced tensile strength and elongation at break. On the other hand, the introduction of more CNT/GNP hybrids increases the filler–filler and filler–polymer networks, which further reinforce the composites and resists the removal of polymer chains; this results in improved tensile strength and decreased elongation at break. The Young’s modulus of ECG0, ECG1, ECG2 and ECG3 are 0.05 GPa, 0.051 GPa, 0.052 GPa and 0.057 GPa, respectively. Besides, the shore A hardness of ECG0, ECG1, ECG2 and ECG3 are 79, 81, 82 and 84. The Young’s modulus and the hardness of the CNT/GNP/EUG composite show a slight increase with the increase in the CNT/GNP hybrids, an indication of the reinforcement of CNT/GNP hybrids. ECG3 exhibits a tensile strength of 20.9 MPa and elongation at a break of 304%. Therefore, the combination of the excellent electromagnetic shielding performance and high mechanical properties makes the as-prepared CNT/GNP/EUG composite appropriate for a wide range of applications.

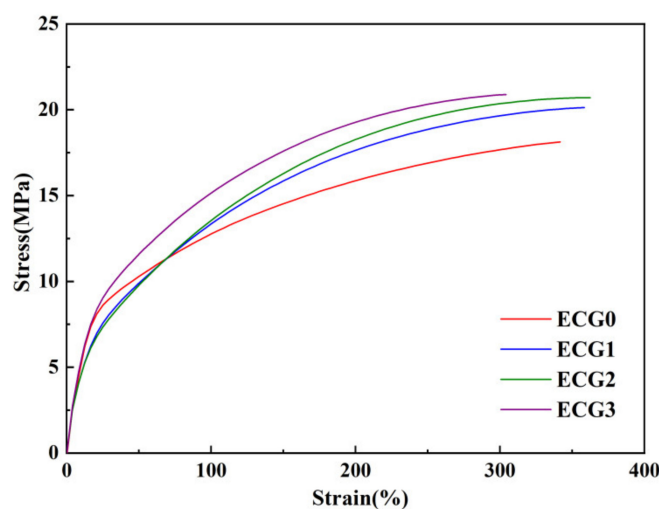


Figure 11. Stress-strain curves of CNT/GNP/EUG composites.

4. Conclusions

In summary, we have successfully fabricated bio-based composites with a high EMI SE and attractive mechanical properties by combining a matrix of EUG with a crystalline structure and CNT/GNP hybrid structures used as conductive fillers. The synergistic effect of the CNT/GNP hybrid originates from the bridging of CNTs between GNPs, which facilitates the enhanced filler networks, electrical conductivity, EMI shielding properties and mechanical properties of the CNT/GNP/EUG composites. The maximum electrical conductivity and EMI SE values of CNT/GNP/EUG composites are observed to be up to 2.71 S/cm and 42.49 dB, respectively. Furthermore, the tensile strength of the CNT/GNP/EUG composites was found to increase with an increase in the GNP loading of the CNT/GNP hybrids. These results indicate that the method studied here provides a practical and effective route towards the creation of high-performance EUG-based EMI shielding composites.

Author Contributions: Conceptualization, H.K., Q.F. and L.L.; methodology, L.L., S.L., H.D. and L.H.; formal analysis, D.L.; investigation, S.L. and H.D.; resources, H.K.; data curation, S.L. and L.H.; writing—original draft preparation, L.L.; writing—review and editing, D.L. and H.K.; supervision, Q.F.; project administration, H.K.; funding acquisition, H.K. and Q.F. All authors have read and agreed to the published version of the manuscript.

Funding: This work was supported by the National Natural Science Foundation of China (grant number 52073178); Natural Science Foundation of Liaoning, China (grant number 2019-MS-263); and Outstanding Young Talent Projects of the Shenyang University of Chemical Technology, China (grant number 2019YQ003).

Informed Consent Statement: Informed consent was obtained from all subjects involved in the study.

Conflicts of Interest: The authors declare no conflict of interest.

References

- Cheng, H.; Wei, S.; Ji, Y.; Zhai, J.; Zhang, X.; Chen, J.; Shen, C. Synergetic effect of Fe₃O₄ nanoparticles and carbon on flexible poly (vinylidene fluoride) based films with higher heat dissipation to improve electromagnetic shielding. *Compos. Part A Appl. Sci. Manuf.* **2019**, *121*, 139–148. [[CrossRef](#)]
- Wu, J.L.; Zhang, Y.R.; Gong, Y.Z.; Wang, K.; Chen, Y.; Song, X.P.; Lin, J.; Shen, B.Y.; He, S.J.; Bian, X.M. Analysis of the electrical and thermal properties for magnetic Fe₃O₄ coated SiC filled epoxy composites. *Polymers* **2021**, *13*, 3028. [[CrossRef](#)] [[PubMed](#)]
- Araby, S.; Meng, Q.; Zhang, L.; Kang, H.; Majewski, P.; Tang, Y.; Ma, J. Electrically and thermally conductive elastomer/graphene nanocomposites by solution mixing. *Polymer* **2014**, *55*, 201–210. [[CrossRef](#)]
- Li, X.H.; Li, X.; Liao, K.N.; Min, P.; Liu, T.; Dasari, A.; Yu, Z.Z. Thermally Annealed Anisotropic Graphene Aerogels and Their Electrically Conductive Epoxy Composites with Excellent Electromagnetic Interference Shielding Efficiencies. *ACS Appl. Mater. Interfaces* **2016**, *8*, 33230–33239. [[CrossRef](#)]

5. Zhai, S.X.; Dai, W.X.; Lin, J.; He, S.J.; Zhang, B.; Chen, L. Enhanced proton conductivity in sulfonated poly(ether ether ketone) membranes by incorporating sodium dodecyl benzene sulfonate. *Polymers* **2019**, *11*, 203. [[CrossRef](#)]
6. Zhan, Y.; Wang, J.; Zhang, K.; Meng, Y.; Yan, N.; Wei, W.; Peng, F.; Xia, H. Fabrication of a flexible electromagnetic interference shielding Fe₃O₄@reduced graphene oxide/natural rubber composite with segregated network. *Chem. Eng. J.* **2018**, *344*, 184–193. [[CrossRef](#)]
7. Li, Y.; Shen, B.; Pei, X.; Zhang, Y.; Yi, D.; Zhai, W.; Zhang, L.; Wei, X.; Zheng, W. Ultrathin carbon foams for effective electromagnetic interference shielding. *Carbon* **2016**, *100*, 375–385. [[CrossRef](#)]
8. Sun, R.; Zhang, H.B.; Liu, J.; Xie, X.; Yang, R.; Li, Y.; Hong, S.; Yu, Z.Z. Highly Conductive Transition Metal Carbide/Carbonitride(MXene)@polystyrene Nanocomposites Fabricated by Electrostatic Assembly for Highly Efficient Electromagnetic Interference Shielding. *Adv. Funct. Mater.* **2017**, *27*, 1702807–1702818. [[CrossRef](#)]
9. He, S.J.; Dai, W.X.; Yang, W.; Liu, S.X.; Bian, X.M.; Zhang, C.; Lin, J. Nanocomposite proton exchange membranes based on phosphotungstic acid immobilized by polydopamine-coated halloysite nanotubes. *Polym. Test.* **2019**, *73*, 242–249. [[CrossRef](#)]
10. He, S.J.; Wang, J.Q.; Yu, M.X.; Xue, Y.; Hu, J.B.; Lin, J. Structure and mechanical performance of poly(vinyl alcohol) nanocomposite by incorporating graphitic carbon nitride nanosheets. *Polymers* **2019**, *11*, 610. [[CrossRef](#)]
11. Guo, Y.; Xu, G.; Yang, X.; Ruan, K.; Ma, T.; Zhang, Q.; Gu, J.; Wu, Y.; Liu, H.; Guo, Z. Significantly enhanced and precisely modeled thermal conductivity in polyimide nanocomposites with chemically modified graphene via in situ polymerization and electrospinning-hot press technology. *J. Mater. Chem. C* **2018**, *6*, 3004–3015. [[CrossRef](#)]
12. Liao, Y.F.; Weng, Y.X.; Wang, J.Q.; Zhou, H.F.; Lin, J.; He, S.J. Silicone rubber composites with high breakdown strength and low dielectric loss based on polydopamine coated mica. *Polymers* **2019**, *11*, 2030. [[CrossRef](#)] [[PubMed](#)]
13. Liu, H.; Xu, Y.; Cao, J.; Han, D.; Yang, Q.; Li, R.; Zhao, F. Skin structured Silver/Three-dimensional Graphene/Polydimethylsiloxane Composites with Exceptional Electromagnetic Interference Shielding Effectiveness. *Compos. Part A Appl. Sci. Manuf.* **2021**, *148*, 106476–106507. [[CrossRef](#)]
14. Arjmand, M.; Chizari, K.; Krause, B.; Petra, P.; Uttandaraman, S. Effect of synthesis catalyst on structure of nitrogen-doped carbon nanotubes and electrical conductivity and electromagnetic interference shielding of their polymeric nanocomposites. *Carbon* **2016**, *98*, 358–372. [[CrossRef](#)]
15. He, S.J.; Wang, J.Q.; Hu, J.B.; Zhou, H.F.; Nguyen, H.; Luo, C.M.; Jun Lin, J. Silicone rubber composites incorporating graphitic carbon nitride and modified by vinyl tri-methoxysilane. *Polym. Test.* **2019**, *79*, 106005. [[CrossRef](#)]
16. Bian, X.M.; Tuo, R.; Yang, W.; Zhang, Y.R.; Xie, Q.; Zha, J.W.; Lin, J.; He, S.J. Mechanical, thermal, and electrical properties of BN-epoxy composites modified with carboxyl-terminated butadiene nitrile liquid rubber. *Polymers* **2019**, *11*, 1548. [[CrossRef](#)] [[PubMed](#)]
17. Zhang, J.; Zhang, H.; Wang, H.; Chen, F.; Zhao, Y. Extruded conductive silicone rubber with high compression recovery and good aging-resistance for electromagnetic shielding applications. *Polym. Compos.* **2019**, *40*, 1078–1086. [[CrossRef](#)]
18. Park, D.H.; Lee, Y.K.; Park, S.S.; Lee, C.S.; Kim, S.H.; Kin, W.N. Effects of hybrid fillers on the electrical conductivity and EMI shielding efficiency of polypropylene/conductive filler composites. *Macromol. Res.* **2013**, *21*, 905–910. [[CrossRef](#)]
19. Avi, B.; Eric, M.; Alan, T. Comparison of Experimental and Modeled EMI Shielding Properties of Periodic Porous xGNP/PLA Composites. *Polymers* **2019**, *11*, 1233.
20. Rahaman, M.; Chaki, T.K.; Khashtgir, D. Development of high performance EMI shielding material from EVA, NBR, and their blends: Effect of carbon black structure. *J. Mater. Sci.* **2011**, *46*, 3989–3999. [[CrossRef](#)]
21. Maria, G.P.C.; Maxime, B.; Can, K.; Anastasios, C.M.; Nikolaos, K.; Gian, P.P.; Antonello, A.; Ernesto, D.M.; Costas, G. Thermoplastic polyurethane-graphene nanoplatelets microcellular foams for electromagnetic interference shielding. *Graphene Technol.* **2020**, *5*, 33–39.
22. Yim, Y.J.; Park, S.J. Electromagnetic interference shielding effectiveness of high-density polyethylene composites reinforced with multi-walled carbon nanotubes. *J. Ind. Eng. Chem.* **2015**, *21*, 155–157. [[CrossRef](#)]
23. Rollo, G.; Ronca, A.; Cerruti, P.; Gan, X.P.; Fei, G.X.; Xia, H.S.; Gorokhov, G.; Bychanok, D.; Kuzhir, P.; Lavorgna, M.; et al. On the Synergistic Effect of Multi-Walled Carbon Nanotubes and Graphene Nanoplatelets to Enhance the Functional Properties of SLS 3D-Printed Elastomeric Structures. *Polymers* **2020**, *12*, 1841. [[CrossRef](#)] [[PubMed](#)]
24. Cheng, H.; Cao, C.; Zhang, Q.; Wang, Y.; Liu, Y.; Huang, B.; Sun, X.L.; Guo, Y.; Xiao, L.; Chen, Q.; et al. Enhancement of Electromagnetic Interference Shielding Performance and Wear Resistance of the UHMWPE/PP Blend by Constructing a Segregated Hybrid Conductive Carbon Black-Polymer Network. *ACS Omega* **2021**, *6*, 15078–15088. [[CrossRef](#)]
25. Lin, C.W.; Lou, C.W.; Huang, C.H.; Huang, C.L.; Lin, J.H. Electromagnetically shielding composite made from carbon fibers, glass fibers, and impact-resistant polypropylene: Manufacturing technique and evaluation of physical properties. *J. Thermoplast. Compos. Mater.* **2014**, *27*, 1451–1460. [[CrossRef](#)]
26. Wu, N.; Qiao, J.; Liu, J.; Du, W.; Xu, D.; Liu, W. Strengthened electromagnetic absorption performance derived from synergistic effect of carbon nanotube hybrid with Co@C beads. *Adv. Compos. Hybrid Mater.* **2017**, *1*, 149–159. [[CrossRef](#)]
27. Wang, L.; Wu, Y.; Wang, Y.; Li, H.; Jiang, N.; Niu, K. Laterally Compressed Graphene Foam/Acrylonitrile Butadiene Styrene Composites for Electromagnetic Interference Shielding. *Compos. Part A Appl. Sci. Manuf.* **2020**, *133*, 105887. [[CrossRef](#)]
28. Anooja, J.B.; Dijith, K.S.; Surendran, K.P.; Subodh, G. A simple strategy for flexible electromagnetic interference shielding: Hybrid rGO@CB-Reinforced polydimethylsiloxane. *J. Alloy. Compd.* **2019**, *807*, 151678. [[CrossRef](#)]

29. Li, Y.; Pei, X.; Shen, B.; Zhai, W.; Zhang, L.; Zhen, W. Polyimide/graphene composite foam sheets with ultrahigh thermostability for electromagnetic interference shielding. *RSC Adv.* **2015**, *5*, 24342–24351. [[CrossRef](#)]
30. Li, Y.; Xu, F.; Lin, Z.; Sun, X.; Peng, Q.; Yuan, Y.; Wang, S.; Yang, Z.; He, X.; Li, Y. Electrically and thermally conductive underwater acoustically absorptive graphene/rubber nanocomposites for multifunctional applications. *Nanoscale* **2017**, *9*, 14476–14485. [[CrossRef](#)]
31. Al-Ghamdi, A.A.; Al-Ghamdi, A.A.; Al-Turki, Y.; El-Tantawy, F. Electromagnetic shielding properties of graphene/acrylonitrile butadiene rubber nanocomposites for portable and flexible electronic devices. *Compos. Part B Eng.* **2016**, *88*, 212–219. [[CrossRef](#)]
32. Wu, H.Y.; Zhang, Y.P.; Jia, L.C.; Yan, D.X.; Gao, J.F.; Li, Z.M. Injection Molded Segregated Carbon Nanotube/Polypropylene Composite for Efficient Electromagnetic Interference Shielding. *Ind. Eng. Chem. Res.* **2018**, *57*, 12378–12385. [[CrossRef](#)]
33. Abraham, J.; Arif, P.M.; Xavier, P.; Bose, S.; George, S.C.; Kalarikkal, N.; Thomas, S. Investigation into dielectric behaviour and electromagnetic interference shielding effectiveness of conducting styrene butadiene rubber composites containing ionic liquid modified MWCNT. *Polymer* **2017**, *112*, 102–115. [[CrossRef](#)]
34. Lu, S.; Bai, Y.; Wang, J.; Chen, D.; Ma, K.; Meng, Q.; Liu, X. Flexible GNPs/EPDM with Excellent Thermal Conductivity and Electromagnetic Interference Shielding Properties. *Nano* **2019**, *14*, 1950075. [[CrossRef](#)]
35. Gupta, S.; Tai, N.H. Carbon materials and their composites for electromagnetic interference shielding effectiveness in X-band. *Carbon* **2019**, *152*, 159–187. [[CrossRef](#)]
36. Guo, Y.; Pan, L.; Yang, X.; Ruan, K.; Han, Y.; Kong, J.; Gu, J. Simultaneous improvement of thermal conductivities and electromagnetic interference shielding performances in polystyrene composites via constructing interconnection oriented networks based on electrospinning technology. *Compos. Part A Appl. Sci. Manuf.* **2019**, *124*, 105484–105522. [[CrossRef](#)]
37. Sun, H.; Chen, D.; Ye, C.; Li, X.; Dai, D.; Yuan, Q.; Chee, K.; Zhao, P.; Jiang, N.; Lin, C.T. Large-area self-assembled reduced graphene oxide/electrochemically exfoliated graphene hybrid films for transparent electrothermal heaters. *Appl. Surf. Sci.* **2018**, *435*, 809–814. [[CrossRef](#)]
38. Huangfu, Y.; Ruan, K.; Qiu, H.; Lu, Y.; Liang, C.; Kong, J.; Gu, J. Fabrication and investigation on the PANI/MWCNT/thermally annealed graphene aerogel/epoxy electromagnetic interference shielding nanocomposites. *Compos. Part A Appl. Sci. Manuf.* **2019**, *121*, 265–272. [[CrossRef](#)]
39. Zhao, S.; Yan, Y.; Gao, A.; Zhao, S.; Cui, J.; Zhang, G. Flexible Polydimethylsilane Nanocomposites Enhanced with a Three-Dimensional Graphene/Carbon Nanotube Bicontinuous Framework for High-Performance Electromagnetic Interference Shielding. *ACS Appl. Mater. Interfaces* **2018**, *10*, 26723–26732. [[CrossRef](#)]
40. Kim, M.S.; Yan, J.; Joo, K.H.; Pandey, J.K.; Kang, Y.J.; Ahn, S.H. Synergistic effects of carbon nanotubes and exfoliated graphite nanoplatelets for electromagnetic interference shielding and soundproofing. *J. Appl. Polym. Sci.* **2013**, *130*, 3947–3951. [[CrossRef](#)]
41. Mohammed, H.; Al, S. Electrical, EMI shielding and tensile properties of PP/PE blends filled with GNP:CNT hybrid nanofiller. *Synth. Met.* **2016**, *217*, 322–330.
42. Güler, Ö.; Başgöz, Ö.; Güler, S.H.; Canbay, C.A.; Açıkgöz, Ş.; Boyrazlı, M. The synergistic effect of GNPs+CNTs on properties of polyester: Comparison with polyester–CNTs nanocomposite. *J. Mater. Sci. Mater. Electron.* **2021**, *32*, 17436–17447. [[CrossRef](#)]
43. Wang, Y.; Wang, W.; Qi, Q.; Xu, N.; Yu, D. Layer-by-layer assembly of PDMS-coated nickel ferrite/multiwalled carbon nanotubes/cotton fabrics for robust and durable electromagnetic interference shielding. *Cellulose* **2020**, *27*, 2829–2845. [[CrossRef](#)]
44. Shen, B.; Li, Y.; Yi, D.; Zhai, W.; Wei, X.; Zheng, W. Strong flexible polymer/graphene composite films with 3D saw-tooth folding for enhanced and tunable electromagnetic shielding. *Carbon* **2017**, *113*, 55–62. [[CrossRef](#)]
45. Wang, G.; Liao, X.; Yang, J.; Tang, W.; Zhang, Y.; Jiang, Q.; Li, G. Frequency-selective and tunable electromagnetic shielding effectiveness via the sandwich structure of silicone rubber/graphene composite. *Compos. Sci. Technol.* **2019**, *184*, 107847. [[CrossRef](#)]
46. Liu, W.; Liu, J.; Yang, Z.; Ji, G. Extended working frequency of ferrites by synergistic attenuation through a controllable carbothermal route based on prussian blue shell. *ACS Appl. Mater. Interfaces* **2018**, *10*, 28887–28897. [[CrossRef](#)]
47. Vovchenko, L.; Matzui, L.; Oliynyk, V.; Launets, V.; Mamunya, Y.; Maruzhenko, O. Nanocarbon/polyethylene composites with segregated conductive network for electromagnetic interference shielding. *Mol. Cryst. Liq. Cryst.* **2019**, *672*, 186–198. [[CrossRef](#)]
48. Xia, T.; Zhang, C.; Oyler, N.A.; Chen, X. Hydrogenated TiO₂ nanocrystals: A novel microwave absorbing material. *Adv. Mater.* **2013**, *25*, 6905–6910. [[CrossRef](#)]
49. Dong, J.Y.; Ullal, R.; Han, J.; Wei, S.; Ouyang, X.; Dong, J.; Dong, J.Z.; Gao, W. Partially crystallized TiO₂ formicrowave absorption. *J. Mater. Chem. A* **2015**, *3*, 5285–5288. [[CrossRef](#)]